Supporting Information

Construction of Nanocage-Structured Heterogeneous Binary Metal Sulfides via Step-by-Step Confined Growth for Boosted Lithium Storage Properties

Rongfang Zhao[a,b], Yue Han[c], Wenlong Li[c], Jinhua Li[a,b], Ming Chen*[c], Lingxin Chen*[a,b]

[a] Institute of Oceanology, Chinese Academy of Sciences, Qingdao 266071

[b] Key Laboratory of Coastal Environmental Processes and Ecological Remediation, Yantai Institute of Coastal Zone Research, Chinese Academy of Sciences, Yantai 264003

[c] School of Chemistry and Chemical Engineering, Yangzhou University, Yangzhou 225002, Jiangsu, China

Email: chenming@yzu.edu.cn (M. Chen); lxchen@yic.ac.cn (L.X. Chen)

Experimental Section

Synthesis of nanocage-structured MoS_2@CNCs

Carbon nanocages (CNCs) were synthesized according to the previously reported method. 100 mg $Na_2MoO_4 \cdot 2H_2O$ and 300 mg $CS(NH_2)_2$ added to the suspension solution forming of CNCs dispersed in 25 mL deionized water with homogeneous dispersion. The solution was heated at 120 °C for 6 h after transferring to a 50 mL Teflon-lined stainless-steel autoclave. Then, the solution was centrifugated for collecting and washed with deionized water and ethanol after cooling to room temperature. Lastly, the sample was dried at 60 °C in vacuum overnight to obtain nanocages structure MoS_2@CNCs.

Synthesis of nanocage-structured Co_9S_8/MoS_2@CNCs

A certain amount of $Co(NO_3)_2 \cdot 6H_2O$ and 2-methylimidazole were added into MoS_2@CNCs/methanol solution obtaining by MoS_2@CNCs dispersed in 25 ml methanol solution. The solid mixture was centrifugated and washed three times to obtain nanocage structured ZIF-67/MoS_2@CNCs. ZIF-67/MoS_2@CNCs and sulfur powder were placed on both sides of the quartz boat at a mass ratio of 1:1, and then the mixture was heated to 800 °C in Ar for 2 h giving nanocage-structured Co_9S_8/MoS_2@CNCs.The nanocage-structure Co_9S_8@CNCs were obtained by using CNCs as presoma replacing the MoS_2@CNCs in the 2.2 section.

Materials characterization

Field-emission scanning electron microscopy (FESEM) was carried out with Hitachi S-4800 (Japan). Transmission Electron Microscopy (TEM) was conducted on

JEOL JEM-2100 instrument. High-resolution TEM (HRTEM) and high-angle annular dark-field scanning transmission electron microscopy (HAADF-STEM) were performed on FEI Tecnai G2 F30 STWIN (USA) operating at 300 kV. X-ray diffraction (XRD) data were obtained with a graphite monochromator and Cu K radiation (λ= 0.1541 nm) on D8 advance superspeed powder diffractometer (Bruker). Raman spectra were carried out on Renishaw via Raman spectroscope. X-ray photoelectron spectroscopy (XPS) were conducted by Thermo Escalab 250 system using Al Ka radiation (hv = 1486.6 eV), the pressure of test chamber was maintained below 2□10-9 Torr during spectral acquisition. Thermogravimetry analysis (TGA, Pyris 1 TGA, PerkinElmer, USA) data were obtained in air. Surface areas and pore size distributions were recorded by BET technique in an automated surface area and porosity analyzer (ASAP 2020, HD88) at -196 ^{o}C after samples being dried at 100 ^{o}C for 4 h.

Electrochemical tests

Anode electrodes were prepared by mixing the nanocage-structure Co_9S_8/MoS_2@CNCs, Co_9S_8@CNCs, or MoS_2@CNCs (80%) with 10 % acetylene black as a conductive material, and 10 % polyvinylidene difluoride (PVDF) binder dissolved in N-methyl-2-pyrrolidinone (NMP). Then, the slurries were cast onto a copper foil current collector. After coating, the electrodes were dried at 80 °C for 10 h to remove the solvent before pressing. The electrodes were punched in the form of disks and then vacuumdried at 120 °C for 12 h. And then the button cells (CR 2032 coin-type cell) were assembled with metallic lithium as the counter/reference electrode, 1 M $LiPF_6$ in EC/DMC/EMC (1:1:1 by volume) is used as electrolyte, and Celgard 2400 polypropylene as separator in a high-purity argonfilled glovebox (Vacuum Atmospheres Co., Ltd).

Cyclic voltammetry (CV) measurements were performed using an electrochemicalworkstation (CHI660 E, Chenghua, CHN) at a scan rate of 0.1 mV s^{-1} between 0.001 and 3.0 V. Electrochemical impedance spectroscopic (EIS) experiments were performed with Autolab Electrochemical Analyzer (Ecochemie, Netherlands). Galvanostatic charge (lithium insertion) and discharge (lithium extraction) cycles of the cells were carried out using a battery test system (CT-3008W, Xinwei, CHN) at various current densities between 0.001 and 3 V (*vs.* Li^+/Li) to determine rate performance, and to evaluate cycle stability at the current density of 0.5 A g^{-1}.

Figure Captions

Figure S1 (a) SEM and (b) TEM images of CNCs.

Figure S2 (a) SEM and (b) TEM images of ZIF-67.

Figure S3 SEM images Co_9S_8/MoS_2@CNCs.

Figure S4 BET spectra of Co_9S_8/MoS_2@CNCs.

Figure S5 (a) SEM and (b) TEM images of Co_9S_8@CNCs.

Figure S6 TGA curves of Co_9S_8@CNCs and Co_9S_8/MoS_2@CNCs.

Figure S7 TGA curves of MoS_2@CNCs.

Figure S8 Raman spectra of Co_9S_8@CNCs and Co_9S_8/MoS_2@CNCs.

Figure S9 XPS survey spectrum of the Co_9S_8/MoS_2@CNCs.

Figure S10 XPS survey spectrum of the Co_9S_8@CNCs.

Figure S11 Cycling performance at 0.2 A g^{-1} of Co_9S_8@CNCs.

Figure S12 Cycling performance at 0.2 A g^{-1} of CNCs.

Figure S13 TEM and HRTEM images of Co_9S_8/MoS_2@CNCs after 1000 cycles at 2 A g^{-1}.

Figure S14 Z'plotted against $\omega^{-1/2}$ at low frequency region for Co_9S_8/MoS_2@CNFs, Co_9S_8@CNCs, and MoS_2@CNCs.

Table S1 R_{ct}, σ and D_{Li} of Co_9S_8/MoS_2@CNFs, Co_9S_8@CNCs, and MoS_2@CNCs.

Table S2 Summary of electrochemical performances of different Co_9S_8/MoS_2-based, MoS_2-based or Co_9S_8-based anodes.

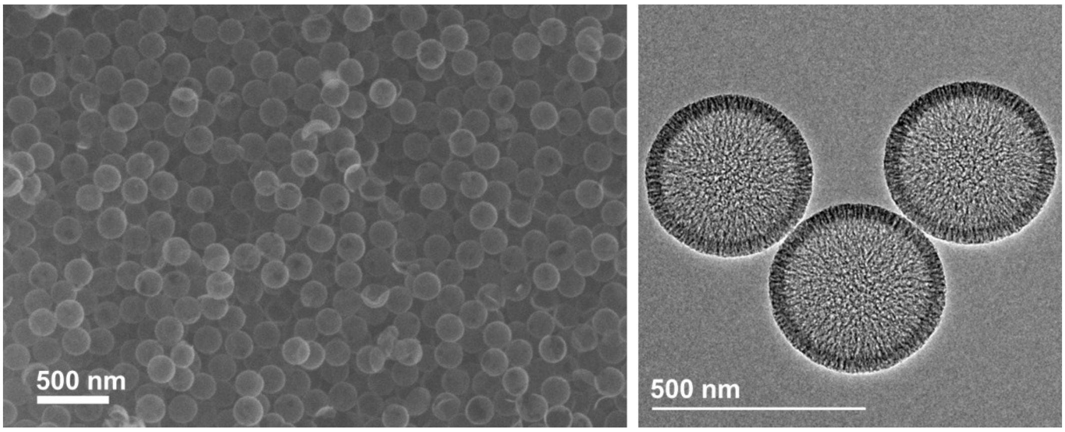

Figure S1 SEM and TEM images of CNCs.

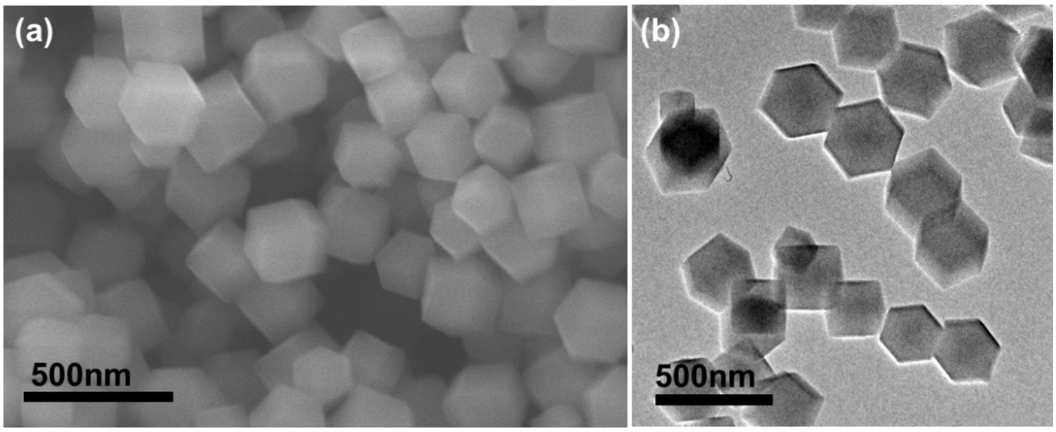

Figure S2 (a) SEM and (b) TEM images of ZIF-67.

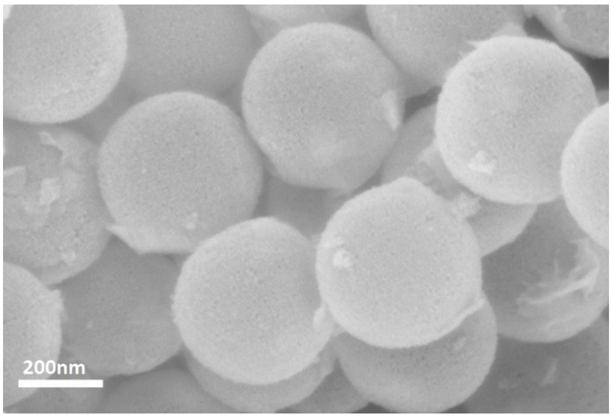

Figure S3 SEM images Co_9S_8/MoS_2@CNCs.

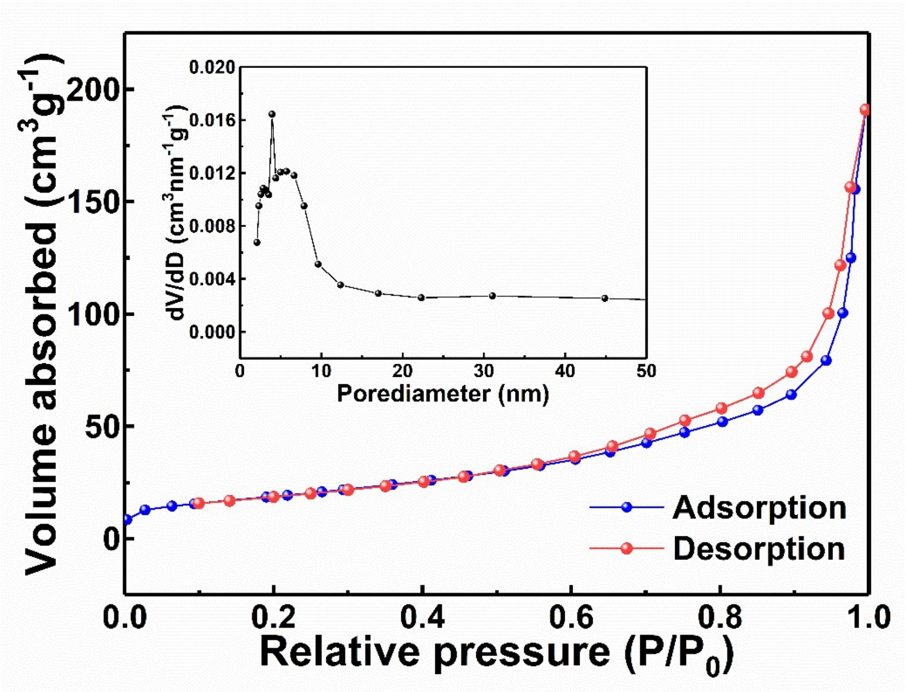

Figure S4 BET spectra of Co_9S_8/MoS_2@CNCs.

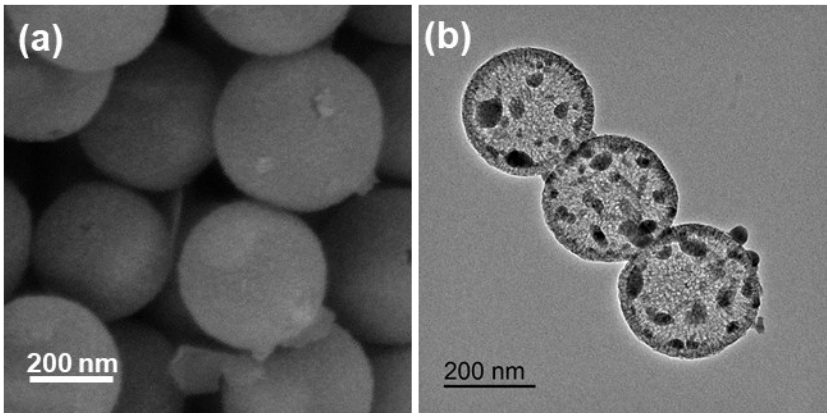

Figure S5 (a) SEM and (b) TEM images of Co_9S_8@CNCs.

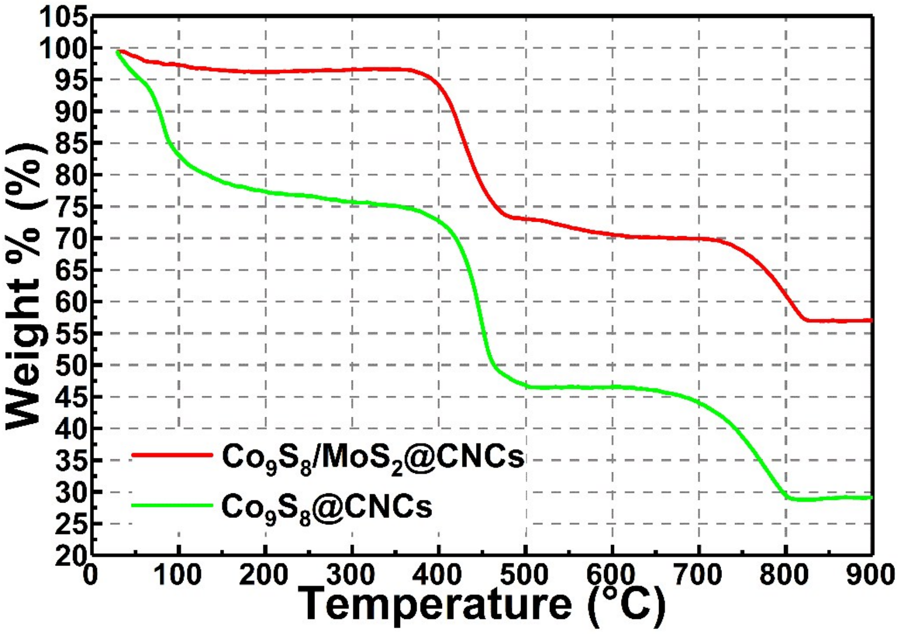

Figure S6 TGA curves of Co_9S_8@CNCs and Co_9S_8/MoS_2@CNCs.

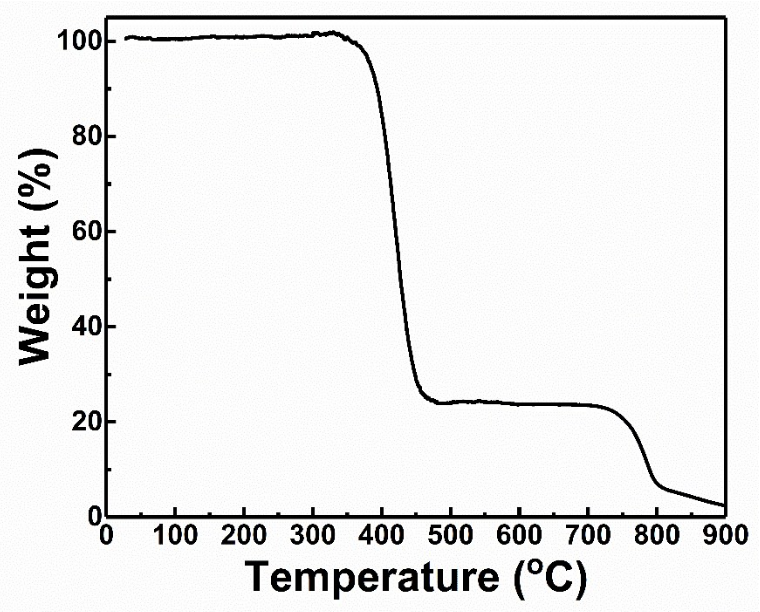

Figure S7 TGA curves of MoS_2@CNCs.

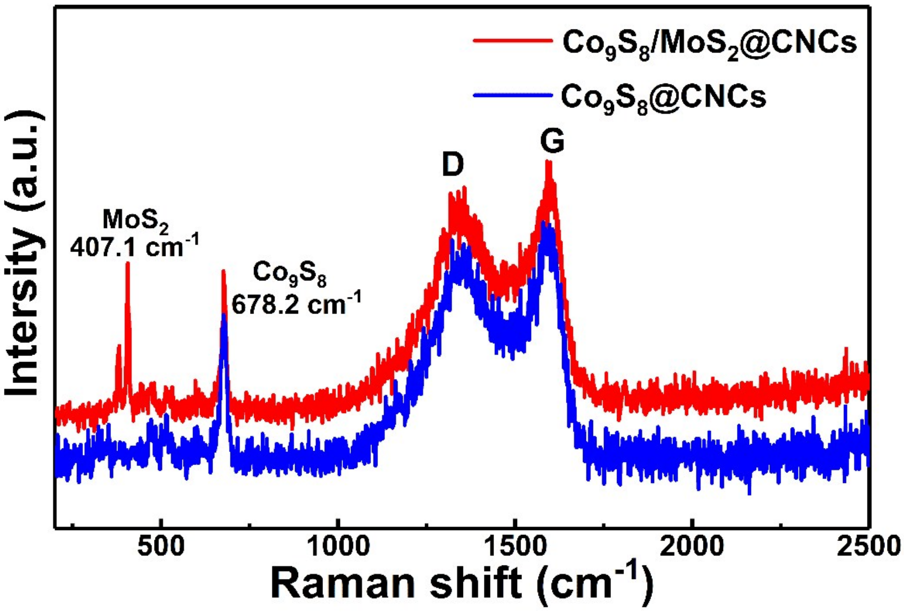

Figure S8 Raman spectra of Co$_9$S$_8$/MoS$_2$@CNCs and Co$_9$S$_8$@CNCs.

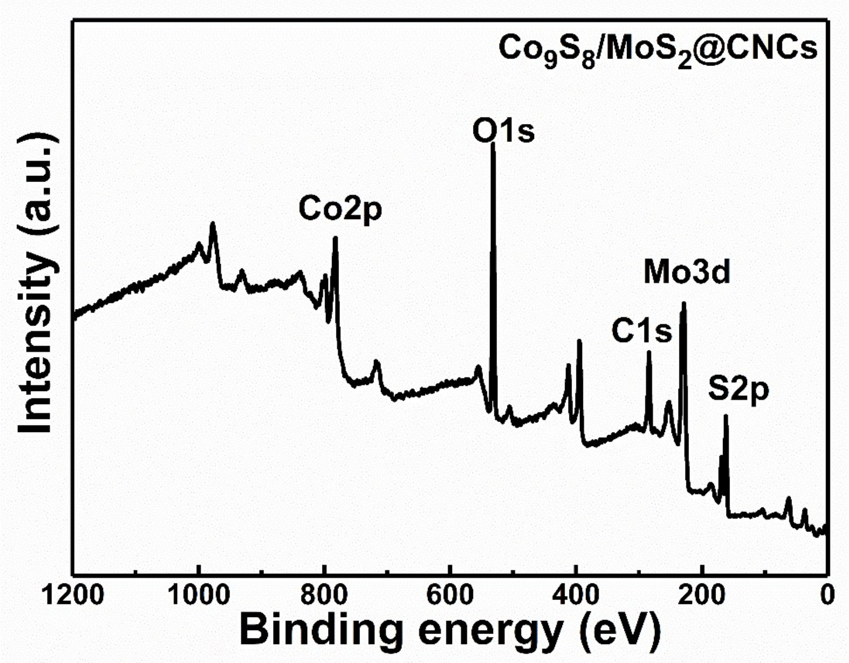

Figure S9 XPS survey spectrum of the Co$_9$S$_8$/MoS$_2$@CNCs.

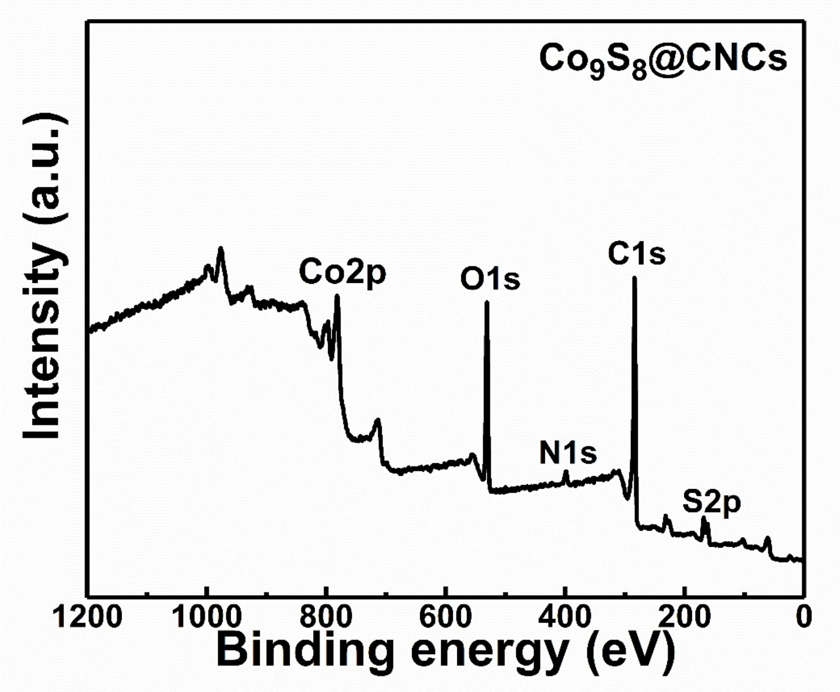

Figure S10 XPS survey spectrum of the Co_9S_8@CNCs.

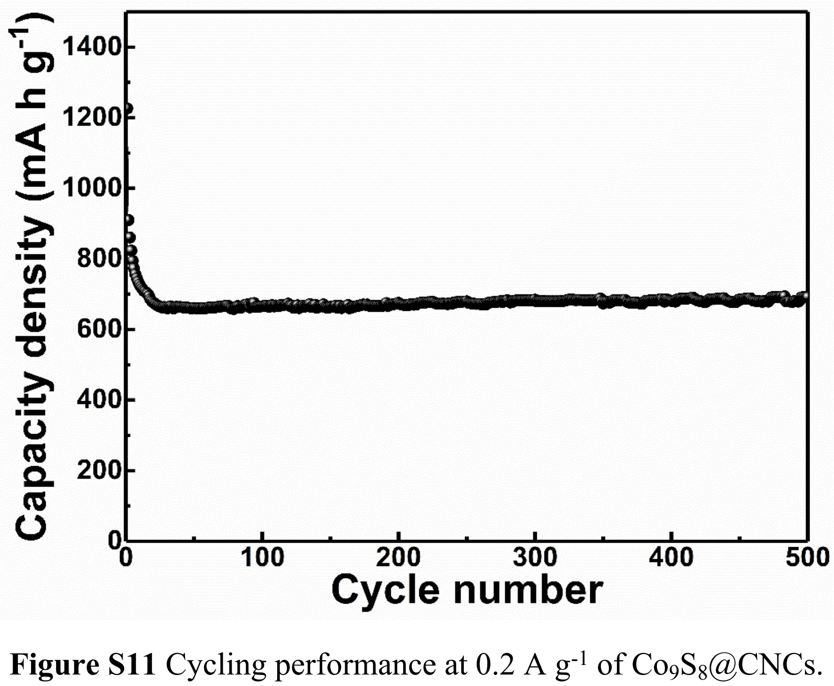

Figure S11 Cycling performance at 0.2 A g^{-1} of Co_9S_8@CNCs.

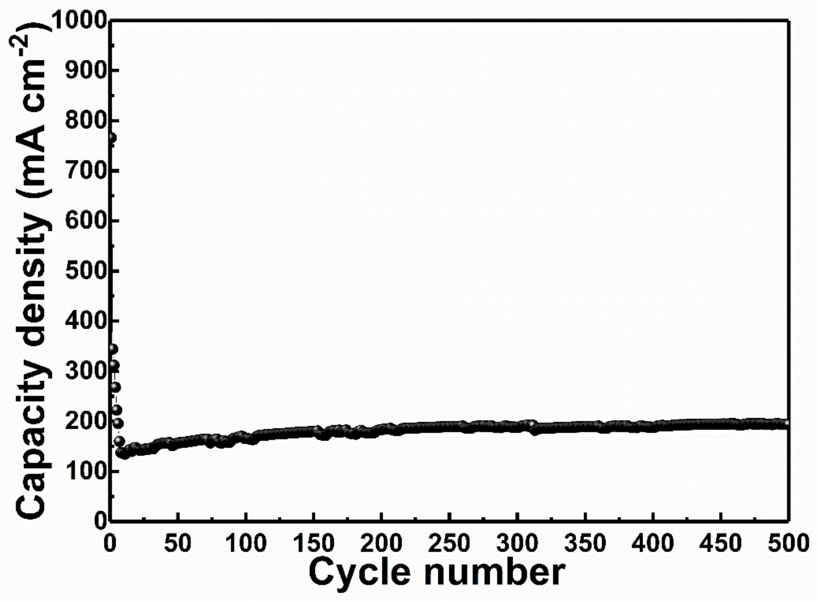

Figure S12 Cycling performance at 0.2 A g^{-1} of CNCs.

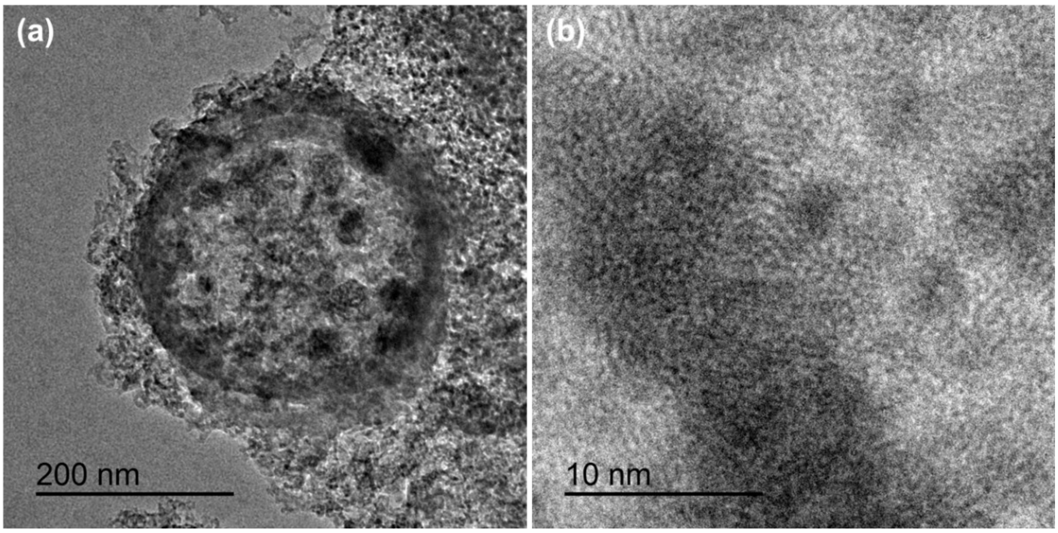

Figure S13 TEM and HRTEM images of Co_9S_8/MoS_2@CNCs after 1000 cycles at 2 A g^{-1}.

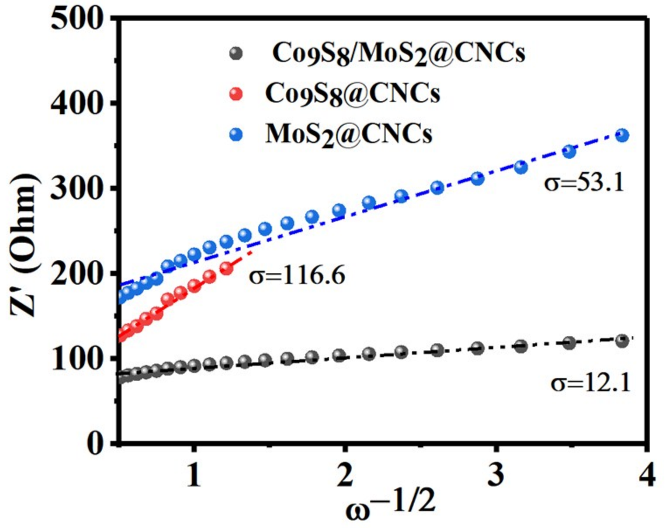

Figure S14 Z' plotted against $\omega^{-1/2}$ at low frequency region for Co_9S_8/MoS_2@CNFs, Co_9S_8@CNCs, and MoS_2@CNCs.

The following equations can be used to calculate the diffusion coefficient of the Li^+ (D_{Li}):

$$Z' = R_s + R_{ct} + \sigma\omega^{-1/2} \quad (1)$$

$$D_{Li} = \frac{R^2T^2}{2A^2n^4F^4c^2\sigma^2} \quad (2)$$

R is the gas constant, T *is* the absolute temperature, A is the electrode area, n represents the electrons number, F is the Faraday constant, c is the lithium ion concentration, and σ shows the Warburg factor obtaining by Figure S14. The values of D_{Li} are shown in Table S1. The Co_9S_8/MoS_2@CNCs display the largest D_{Li}, which reveals Co_9S_8/MoS_2@CNCs have the excellent property of Li-ion diffusion.

Table S1 R_{ct}, σ and D_{Li} of Co_9S_8/MoS_2@CNFs, Co_9S_8@CNCs, and MoS_2@CNCs.

Samples	R_{ct}/Ω	σ	D_{Li}/cm^2 s^{-1}
Co_9S_8/MoS_2@CNCs	67.0	12.1	1.97×10^{-13}
Co_9S_8@CNCs	96.7	116.6	2.12×10^{-15}
MoS_2@CNCs	146.6	53.1	1.02×10^{-14}

Table S2 Summary of electrochemical performances of different Co_9S_8/MoS_2-based, MoS_2-based or Co_9S_8-based anodes.

Sample	**Rate capability (mA h g^{-1})/Current density (A g^{-1})**	**Reversible capacity (mA h g^{-1})/Cycles/Current density (A g^{-1})**	**Reference**
Co_9S_8/MoS_2@CNCs	550.5/5	1014.0/500/0.2 731/1000/2	This work
Co_9S8/MoS_2-CN	275/20.0	438/150/1.0 421/250/2.0	[1]
Co_9S_8@MoS_2 composites	941/2.0	1048/300/1.0	[2]
Co_9S_8@MoS_2/rGO	838.2/5.0	2014.5/200/0.3	[3]
Co_9S_8/MoS_2 yolk shell spheres	562/5.0	732/200/1.0	[4]
hollow MoS_2–carbon nanocomposites	587/1.0	533/70/0.5	[5]
Co_9S_8/N-C@MoS_2 dodecahedral heterogeneous nanocages	560/5	557/400/5	[6]
Co_9S_8/MoS_2 ultrathin nanosheets	784/5	541/200/2	[7]
hollow carbon nanosphere@Co9S8	220/5.0	560/400/1.0	[8]
micro/nanostructured Co_9S_8 cubes and spheres	439/5.0	370/300/1.0	[9]
Co_9S_8 hollow spheres	100.5/0.5	254.9/100/0.1	[10]
MoS_2/polyaniline nanowires	50/1.0	1063.9/50/0.1	[11]
1T-MoS_2/C	600/10.0	870/300/1	
graphene oxide/MoS_2 nanoflowers	678/2.5	680/250/0.5	[12]
graphene/MoS_2 composites	400/2.0	350/100/1.0	[13]
MoS_2 Hollow Nanospheres	576/5	1100/100/0.5	[14]
CNT network–MoS_2 composite	1224/1.0	1535/50/0.2	[15]

honeycomb-like MoS_2	800/5.0	1235.3/60.0.2	16

Reference

1 Y. Wang, W. Kang, D. Cao, M. Zhang, Z. Kang, Z. Xiao, R. Wang and D. Sun, *J. Mater. Chem. A*, 2018, **6**, 4776-4782.

2 K. Yang, T. Mei, Z. Chen, M. Xiong, X. Wang, J. Wang, J. Li, L. Yu, J. Qian and X. Wang, *Nanoscale*, 2020, **12**, 3435-3442.

3 H. Ren, C. Gu, J. Zhao, S. W. Joo and J. Huang, *Applied Surface Science*, 2019, **473**, 918-927.

4 H. Geng, J. Yang, Z. Dai, Y. Zhang, Y. Zheng, H. Yu, H. Wang, Z. Luo, Y. Guo, Y. Zhang, H. Fan, X. Wu, J. Zheng, Y. Yang, Q. Yan and H. Gu, *Small*, 2017, **13**.

5 J. Jin, B. Kim, M. Kim, N. Park, S. Kang, S. M. Lee, H. J. Kim and S. U. Son, *Nanoscale*, 2015, **7**, 11280-11285.

6 Y. Han, W. Li, K. Zhou, X. Wu, H. Wu, X. Wu, Q. Shi, G. Diao and M. Chen, *ChemNanoMat*, 2019, **6**, 132-138.

7 Y. Liu, H. Geng, E. H. Ang, X. Cao, J. Zheng and H. Gu, *Chem. Asian J.*, 2019, **14**, 170-176.

8 J. L. Xu, L. Liu, Y. H. Sun, R. Lu, Z. R. Wang and Q. Sun, *Applied Surface Science*, 2020, **514**, 146092.

9 Y. H. Wang, B. H. Wu, X. Y. He, Y. Y. Zhang, H. Li, Y. Y. Peng, J. Wang and J. B. Zhao, *Electrochim. Acta*, 2017, **230**, 299-307.

10 R. Jin, J. Zhou, Y. Guan, H. Liu and G. Chen, *J. Mater. Chem. A*, 2014, **2**, 13241-13244.

11 L. Yang, S. Wang, J. Mao, J. Deng, Q. Gao, Y. Tang and O. G. Schmidt, *Adv. Mater.*, 2013, **25**, 1180-1184.

12 F. Xiong, Z. Cai, L. Qu, P. Zhang, Z. Yuan, O. K. Asare, W. Xu, C. Lin and L. Mai, *ACS Appl. Mater. Interfaces*, 2015, **7**, 12625-12630.

13 T. Wang, G. Zhao, C. Sun, L. Zhang, Y. Wu, X. Hao and Y. Shao, *Adv. Mater. Interfaces*, 2017, **4**, 1601187.

14 Y. Wang, L. Yu and X. W. Lou, *Angew. Chem. Int. Ed.*, 2016, **55**, 7423-7426.

15 C. Lu, W. W. Liu, H. Li and B. K. Tay, *Chem Commun*, 2014, **50**, 3338-3340.

16 J. Wang, J. Liu, D. Chao, J. Yan, J. Lin and Z. X. Shen, *Adv. Mater.*, 2014, **26**, 7162-7169.